Thermal oxidation of oxynitride films as a strategy to achieve (Sr2Ta2O7)100-x(La2Ti2O7)x based oxide perovskite films with x = 1.65

L. Le Gendre, C. Le Paven, M. Haydoura, R. Benzerga, Florent Marlec, A. Sharaiha, François Cheviré, Franck Tessier, A. Moréac

Thermal oxidation of oxynitride films as a strategy to achieve $(Sr_2Ta_2O_7)_{100-x}(La_2Ti_2O_7)_x$ based oxide perovskite films with x = 1.65

L. Le Gendre[1], C. Le Paven[1], M. Haydoura[1], R. Benzerga[1], F. Marlec[1], A. Sharaiha[1], F. Cheviré[2], F. Tessier[2], A. Moréac[3]

[1] Univ Rennes, CNRS, IETR UMR 6164, 35042 Rennes, France.

[2] Univ Rennes, CNRS, ISCR UMR 6226, 35042 Rennes, France.

[3] Univ. Rennes, CNRS, IPR UMR 6251, 35042 Rennes, France.

Abstract

This study concerns STLTO compounds of the ferroelectric $(Sr_2Ta_2O_7)_{100-x}(La_2Ti_2O_7)_x$ solid solution. The purpose is to produce the STLTO composition x = 1.65 as thin films by thermal oxidation of the corresponding oxynitride composition. Indeed, the combination of an STLTO oxide target with a dioxygen-rich reactive atmosphere during the sputtering deposition leads to Sr-deficient oxide thin films, shifting composition and structure from the perovskite to the tetragonal tungsten bronze type. An alternative synthesis pathway is to first deposit, under nitrogen-rich atmosphere, stoichiometric oxynitride films and produce, by thermal annealing under air, the stoichiometric oxide. For low oxidation temperatures ([550-600°C]), samples remain intact and display an oxide character but still contain a significant amount of nitrogen ; they could be described as intermediate phases containing nitrogen-nitrogen pairs as demonstrated by Raman. Dielectric characteristics of these original film materials are of interest with a tunability value of 26 % at 30 kV/cm (10 kHz).

1. Introduction

$ABO_{3-x}N_x$ ($0 \leq x \leq 3$) oxide and oxynitride perovskite compounds have been of interest to the scientific community for many years. Indeed, they possess remarkable and miscellaneous properties, allowing their use in many fields such as non-toxic pigments [1,2], high-K dielectrics [3,4], visible light active photocatalysts [5,6] or colossal magnetoresistance materials [7]. Depending on the applications, these materials can be prepared in the form of single crystals, powders, ceramics or thin films. The oxide materials targeted presented in this paper show a layered perovskite structure and belong to the $(Sr_2Ta_2O_7)_{100-x}(La_2Ti_2O_7)_x$ solid solution recently developed by our research team [8]. These original materials present interesting

dielectric and ferroelectric properties, especially high tunabilities with potential applications in high frequencies tunable telecommunication devices.

The studied $(Sr_2Ta_2O_7)_{100-x}(La_2Ti_2O_7)_x$ solid solution (hereinafter named as STLTO) combines two layered-type perovskites [9] with dissimilar Curie temperatures (TC): $Sr_2Ta_2O_7$ (STO), with TC = −107°C [10] and $La_2Ti_2O_7$ (LTO), with TC = 1461°C [11]. We have demonstrated the ferroelectric behavior of this new family of compounds in the form of ceramics for compositions ranging from x = 0 to 5. Optimal performances were achieved for the composition x = 1.65: the permittivity value was ε' = 375 with tunability values T = 17.9 % at 4 kV/cm [8] and T = 55 % at 30 kV/cm (10 kHz, room temperature) [12]. The purpose of the present work is to produce this STLTO specific composition as a thin film.

As discussed later in this paper, the combination of a stoichiometric STLTO oxide target with a dioxygen-rich reactive atmosphere during the radio-frequency (rf) magnetron sputtering deposition leads to Sr-deficient (Sr/Ta ≈ 0.55) thin films, shifting composition and structure from a perovskite to a Tetragonal Tungsten Bronze (TTB) type. An alternative synthesis pathway is to first deposit, under nitrogen-rich atmosphere, stoichiometric (Sr/Ta = 1) oxynitride perovskite thin films (hereinafter named as STLTON) and then produce, by thermal annealing under static air, a perovskite oxide-type material with the expected Sr/Ta = 1 ratio and so to avoid the TTB phase formation. As thin films, oxynitride materials present original properties compared to their oxide parents, such as an absorption in the visible domain, with potential application as photocatalysts for overall water-splitting [13,14]. As dielectrics, oxynitride thin films exhibit high permittivities with a potential ferroelectric behavior [15]. As an example, $LaTiO_2N$ and $SrTaO_2N$ films present higher permittivities than those of the corresponding oxide films, $La_2Ti_2O_7$ and $Sr_2Ta_2O_7$ respectively, but with higher dielectric losses [16-19].

So, the original concept presented here is to deposit stoichiometric oxynitride films and anneal them under air in order to keep Sr/Ta equal to 1 and therefore produce stoichiometric oxide films that cannot be achieved by the sputtering of an oxide target even under an oxygencontaining plasma. Long term annealing (4 hours) of oxynitride films were performed at temperatures in the range [450 - 1000°C]. As detailed further, the resulting samples display an oxide character (Band gap Eg ≈ 4.5) but still contain a significant amount of nitrogen ; they could be described as intermediate phases as previously shown by L. Le Gendre *et al.* [20-21] and A. Rachel *et al.* [22] on powder materials. The present article is divided as follows. The deposition of the oxide STLTO and oxynitride STLTON thin films is first presented ; then, the

annealing of oxynitride samples is studied, including their chemical, optical, structural and Raman characterization. Dielectric measurements are finally presented which emphasize very interesting dielectric properties of the original intermediate produced phases.

2. Experimental

1. Oxide target for the sputtering deposition

STLTO and STLTON layers were deposited by sputtering from a home-made oxide target, prepared by solid state reaction and cold uniaxial compaction. The $(Sr_2Ta_2O_7)_{100-x}(La_2Ti_2O_7)_x$ STLTO powder with composition x = 1.65 was synthesized according to the following process: stoichiometric amounts of high purity powders of $SrCO_3$, Ta_2O_5, La_2O_3 and TiO_2 were homogenized in isopropanol for 1 h in an agate mortar and dried at 110°C. The obtained powder was pressed into a pellet using an uniaxial press (5 MPa), then calcined in air for 15 h at 1000°C, milled and calcined again at 1400°C for 15 h. In order to obtain the sputtering target, 74 grams of the synthesized $(Sr_2Ta_2O_7)_{98.35}(La_2Ti_2O_7)_{1.65}$ powder were mixed with an organic binder (Rhodoviol 5% wt.) facilitating the shaping and subsequently the manipulability of the target; afterwards, the powder was compacted under static uniaxial pressure of approximately 35 MPa. The target was then slightly treated at 600°C under air to remove the organic binder and obtain some grain cohesion and avoid a collapse of the target during handling. The θ-2θ XRD diagram of the target is presented in Figure 1 : all diffracted peaks can be indexed in a unit cell isostructural to that $Sr_2Ta_2O_7$ compound (JCPDF 70-0248). EDS analysis of a dedicated sample gives a strontium to tantalum ratio Sr/Ta = 0.98, which confirms the targeted stoichiometry of the STLTO oxide material.

2. Thin films deposition and characterization methods

STLTO and STLTON films were deposited by reactive rf magnetron sputtering (Plassys MP450S) using the home made STLTO target located at 5 cm from the substrate holder. The deposition chamber was pumped down to a base pressure of 10^{-5} Pa ; during deposition, the dynamic pressure was maintained at 2.5 Pa (30 mTorr). Depositions were performed under a reactive atmosphere consisting in $(Ar + O_2)$ or $(Ar + N_2)$ gas for the deposition of STLTO oxide and STLTON films respectively. The percentage (vol.%) of the reactive gas (O_2, N_2) in the sputtering atmosphere was varied from 5 to 75. At each change of this percentage, the target was pre-sputtered before deposition during 4 hours under the same dioxygen/dinitrogen percentage than the one used during the deposition, in order to oxidize/nitride the target surface

and reach a stable state. The rf power was adjusted at PRF = 90 W and the substrate temperature (TS) was fixed at TS = 800°C. Thickness of films was changed by the duration of the deposition.

At each run, films were deposited on two single-crystalline substrates obtained from Crystal GmbH (Berlin, Germany): MgO(001) and conductive niobium-doped (1.4 at.%) $SrTiO_3$(001) (Nb-STO). The latter was used to serve both as substrate and bottom electrode for the dielectric characterization, while MgO serves for the determination of the band-gap by UVVisible transmittance and for the determination of the crystallization.

X-ray diffraction patterns of films (and powders) were obtained using a Rigaku SmartLab diffractometer (Cu Kα1 radiation). Conventional θ-2θ diagrams were recorded at 0.01° intervals with a 2 s count time at each step.

UV-visible transmittance spectra were recorded using a Perkin-Elmer Lambda 20 spectrometer in the 200 – 1100 nm wavelengths range. For each sample, the absorption coefficient α is calculated from the transmittance (T) using the relation $\alpha = (1/t)(\ln(1/T))$, where t is the thickness of the film. The bandgap of the material (Eg) is calculated assuming a direct allowed transition and using the relation $(\alpha h\nu)^2 = h\nu - Eg$, where hν is the photon energy. In the plot of $(\alpha h\nu)^2$ as a function of h□, the extrapolation of the linear region of the plot at zero gives the value of Eg [23].

A Horiba/Jobin-Y micro-raman spectrometer was used to collect unpolarized Raman spectra of the thin films in backscattering geometry at ambient temperature. These Raman measurements have been performed with a laser diode at 532 nm. Optical density filters were used to decrease the laser power to avoid heating at the focus point of the laser on the sample. The spectral dispersion was around 1.5cm^{-1}/pixel.

Energy Dispersive Spectrometry (EDS) was used to investigate the cations and nitrogen relative compositions of samples ; analyses were performed using the Aztek OXFORD software through a Jeol JSM IT100 Scanning Electronic Microscope (SEM) operating at 10 kV. Surface of films and cross-section morphologies for the measurement of the thickness of the films were characterized by the above SEM ; the error on the thickness values from the cross-section observations is estimated as being ± 10 nm.

Low frequency dielectric properties (permittivity ε' and dielectric losses tanδ) were measured by a LCR meter (LCR-819 GWInstek). Experiments were conducted on films deposited on 1.4 at.% Nb-doped $SrTiO_3$ (Nb-STO) substrates deposited in the same run than those on MgO substrates. Measurements were performed on capacitance structures in which the bottom electrode is the conducting Nb:STO substrate whereas 200 nm sputtered silver

serves as the top electrode. Measurements were done at 10 kHz and room temperature ; external DC electric fields (0–310 kV) were applied to point out a possible variation of the permittivity, i.e. tunability (T) defined as $T(\%) = | \varepsilon'_E - \varepsilon'_{E=0} | / \varepsilon'_{E=0}$.

3. Results

1. Oxide STLTO and oxynitride STLTON thin film deposition at x = 1.65

First, in order to obtain directly the oxide composition, a series of film samples was achieved by sputtering the STLTO target under the reactive (Ar + O_2) gas, varying the percentage of O_2 from 5 to 75 $\%O_2$. Thin film samples are presented in Table 1 along with their composition in cations (ratio Sr/Ta), band gaps (Eg) values and thicknesses which are higher than 870 nm.

Films deposited with $\%O_2 \geq 10$ are transparent with band-gap values close to 4.4 eV (Figure 2a for the film deposited with $\%O_2 = 25$ named hereafter as "STLTO as-deposited"). Fringes observed in the transmittance spectrum at high wavelength values arise from interferences at the air/film and film/substrate interfaces and their spacing depend on the thickness of film, as well as its roughness and density. The film deposited with $\%O_2 = 5$ has a band gap value Eg = 3.2 eV and is grey ; this can denote an oxygen deficiency in the sample due to the low percentage of dioxygen used during its deposition.

All oxide films present Sr/Ta ratios in the range 0.53 to 0.55 as can be seen in blue in Figure 3, denoting a systematic major strontium deficiency in films compared to the sputtering target, and so to the expected composition (the quantification of La was not made here because of its very small amount in STLTO with x =1.65 ; we assume the same La-deficiency as Sr in our films). Therefore, the XRD diagrams (Figure 4 for the "STLTO as-deposited" film and Figure S1 for all samples) cannot be indexed based on the $Sr_2Ta_2O_7$ perovskite compound for which the ratio Sr/Ta = 1. Considering Sr/Ta ratio values close to 0.55, we propose to identify the phase in films to the strontium-deficient $Sr_{2.83}Ta_5O_{15}$ compound (PDF 9012069) belonging to the tetragonal tungsten bronze (TTB) family. $Sr_{2.83}Ta_5O_{15}$ is an isotype to the β'-$SrTa_2O_6$ TTB material studied by Kim et al. [24]. The indexation of peaks reveals of an orientation of films along their c-axis. Moreover, no amorphous contribution, such as a large bump between 15 and 35°, can be detected in the XRD patterns which would have been the signature of a compound gathering a Ta and Ti over-stoechiometry consequence of the Sr and La deficiency in films.

The film deposited with $\%O_2 = 5$ exhibits the less intense peaks thus evidencing the lowest crystallization. The films deposited with $\% O_2 = 50$ and 75 show an asymmetry of the

(00l) peaks ; we can consider the existence of a (620) contribution for these samples. We also note that the position of the (00*l*) peaks moves to lower angular values when $\%O_2$ increases, which corresponds to an increasing out-of-plane *c* parameter, as can be seen in Figure 5. This c parameter increase is not linear, a plateau at c ≈ 3.93 Å is reached when $\% O_2 \geq 50$. The tabulated c lattice parameter of $Sr_{2.83}Ta_5O_{15}$ is c = 3.864 Å (PDF 9012069) which denotes a discrepancy with the above experimental value ; this can be due to the crystalline influence of the substrate inducing tensile or compressive strains in thin films.

As a conclusion on this series of samples, the sputtering of the STLTO target by the reactive dioxygen gas has not led to the expected result ; strontium deficient TTB oxide films have been obtained instead of stoichiometric perovskite oxide compounds.

The deposition of films using a reactive dinitrogen gas, producing oxynitride STLTON films, was thus performed by sputtering the same STLTO oxide target and using identical deposition parameters than for the above oxide films but under reactive ($Ar + N_2$) gas with $\%N_2$ ranging from 5 to 75 (Table 2).

The deposited films are orange-brown in agreement with an absorption in the visible range and band gap values close to 2.3 eV (Table 2 and Figure 2b for the film deposited with $\%N_2 = 25$ named hereafter as "STLTON as-deposited"). Nitrogen is detected by EDS analysis, as expected, but the important feature is that Sr/Ta ratios are close to 1 (Table 2), with a significant evolution as seen in Figure 3 : Sr/Ta increases with $\%N_2$ and the value of 1 is attained for $\%N_2 \approx 25$.

XRD diagrams (Figure 4 for the "STLTON as-deposited" film and Figure S2 for all samples) can be indexed according to the isostructural $SrTaO_2N$ compound (JCPDF 79-1311), with clear (00*l*) texturation of films. No evolution of the angular peak positions can be noticed as a function of $\%N_2$, contrary to what was observed for the oxide films (as a function of $\%O_2$) ; for the STLTON "as-deposited" film *c* parameter equals 4.083 Å. Comparison of the diagrams of the STLTON and STLTO "as-deposited" samples (Figure 4) shows that the two sets of peaks (oxynitride vs. oxide) are easily differentiated by XRD analysis.

2. <u>Annealings of STLTON films</u>

Giving the proper cation stoichiometry of the STLTON oxynitride films, annealing of these films was performed as a way to produce stoichiometric oxide films. Annealings were done at various temperatures (T_A = 450, 550, 600, 650 and 1000°C) for 4 h in ambient air ; ramp temperature was 2°C/min for heating and cooling. Annealed samples features, with the

“as-deposited” oxide / oxynitride films and the STLTO pristine powder used for the sputtering target, are presented in Table 3.

EDS analysis of the films before and after annealing (Table 3) underlines that the Sr/Ta ratios remain close to 1 for the different annealing temperatures, with no proven trend. Moreover, nitrogen is detected in all annealed films and is in the range 8.5 – 9.5 at.%, except for the film treated at the highest temperature (T_A = 1000°C) which does not contain nitrogen. Discrepancies in the atomic contents from one annealed film to another are due to the uncertainty of the quantification by the EDS method.

As regards the optical transmittance (Figure S3), the starting oxynitride film shows absorption in the visible range with a band gap Eg = 2.3 eV. Visible absorption persists for the film annealed at T_A = 450°C ; band gap of 2.5 eV is determined. The situation changes radically for T_A higher than 550°C : absorption is observed below 400 nm, band gap values are then all greater than 4.1 eV with a rather large spread of values. Due to extreme degradation of the film after the heat treatment at T_A = 1000°C, transmittance measurement was not performed on it.

XRD analysis (Figure 6) shows that the annealing at T_A = 450°C does not affect the XRD signature of the sample which remains that of an oxynitride and, so, is similar to that of the “STLTON as-deposited” film.

For TA ≥ 550°C, an important decrease in the intensity of peaks is observed along with an offset of the positions towards higher 2θ angular values (Figure 6b). These positions correspond neither to that of the STLTO pristine stoichiometric powder, nor to that of the “STLTO asdeposited” film with a strontium deficiency. Angular positions of the annealed films are at intermediate positions. Thus, three sets of the out-of-plane *c* parameter are highlighted in Figure 7 : $c_{PC} \approx 4.08$ Å for oxynitride compounds (“as-deposited” and annealed at T_A = 450°C), $c_{PC} \approx 3.99$ Å for the other annealed films and $c_{PC} \approx 3.945$ Å for the oxide pristine powder. Moreover, it is observed in XRD that the peak intensities of the annealed films decrease as T_A increases, while maintaining a textured crystallization with the presence of (00*l*) peaks. An amorphization of annealed oxynitride films while keeping a perovskite structure is thus observed, as already reported on partially annealed oxynitride powders [20].

Surface morphologies of annealed samples are visible in Figure S4. At high magnification, the initial "as-deposited" oxynitride film is finely granular with grain sizes below 100 nm. The granularity increases with the annealing temperature. At T_A = 1000°C, the film is very smooth. At low magnifications, we can see that films undergo increasing damage as the annealing temperature increases. At T_A = 550°C and 600°C, we observe the formation of craters

where the film begins to peel off the substrate. This phenomenon is accentuated at T_A = 650°C with the presence of holes where the film has completely taken off from the substrate and, finally at T_A = 1000°C, the film remains only in the state of fragments on the substrate.

Figure 8 presents the Raman spectra, in the [2300 – 2350 cm-1] range, of the MgO substrate on which films are deposited, the "STLTON-as-deposited" film and the STLTON-25 film annealed at 600°C. This sample was chosen for the Raman characterization (and for the dielectric measurements as seen below) because it remains as a quasi-continuous film, maintains a textured growth and a Sr/Ta ratio close to 1.

First of all, we find that no peak is visible in the explored range for the as-deposited oxynitride film. The signal at 2331cm^{-1} detected on MgO corresponds to the presence of N_2 adsorbed molecules [21] on the surface of the substrate. Two signals are observed for the STLTON-25 annealed film : a weakly intense shoulder at 2331 cm^{-1} and an intense signal at 2328 cm^{-1}. The first one corresponds to adsorbed N_2 on the surface of the film, while the second corresponds to N_2 molecules trapped in an oxide matrix as previously reported [21,22,25-27] on partially oxidized oxynitride powders.

Indeed, there is a variety of studies which have examined the thermal stability of oxynitride powders, mainly by thermogravimetric analysis (TGA). Many oxynitrides with a large range of compositions and structures lead to such a dinitrogen-containing phase during the first stage of their oxidation. Specific examples, with their related structure type, are : perovskites ($SrTaO_2N$ [22,28], $LaTiO_2N$ [21], $BaTaO_2N$ [20,28], $SrNbO_2N$ [22,25,28], $LaFeO_{3-x}N_x$ [29], $LaNbON_2$ [27], $SrTi_{1-x}Nb_x(O,N)_3$ [30]), rock salt type (NbO_xN_y [20], TiO_xN_y [20], CrO_xN_y [20]), cuspidine-type ($Y_4Si_2O_7N_2$ [31]), Ruddlesden-Popper type (Sr_2NbO_3N [32]), Fluorite type (bixbyite Zr_2ON_2 [26]) or Spinel (AlO_xN_y [33]). While monitoring by TGA the mass variation related to the oxidation of the starting oxynitride (under air or oxygen-containing atmosphere), one can observe, between the oxynitride and the oxide mass levels a so-called intermediate phase [21-22]. This phase is related to important dinitrogen retention since, depending on the oxynitride chemical composition involved, the N_2 amount, trapped in the oxide lattice, can reach as much as 70% of the initial nitrogen. The Raman signature of this dinitrogen molecule in weak interaction with the oxide lattice has been systematically detected close to 2328 cm^{-1} [21-22,25-28,34]. The presence of N_2 molecules in large quantities leads to a strong amorphization of the original structure (see [20] for example). Furthermore, several XPS studies of the controlled oxidation of large range of oxynitrides have confirmed the conversion of the nitride ions (N_{1s} BE = 397 eV) to nitrogen species with a higher oxidation

state (N_{1s} BE = 403 eV) consistent with the presence of dinitrogen molecules weakly bound to the oxide lattice [20, 27].

In our case, SLTTON thin films annealed in the range [550-650°C] under air present an optical oxide signature (Eg > 4.1 eV), clearly showing that the *2p* states of nitrogen are no longer occupying the top of the valence band as regularly observed when N^{3-} substitutes for O^{2-} within the anionic network of the crystal structure of (oxy)nitrides. This is in agreement with molecular N_2 trapped and weakly bonded within an oxide perovskite-type matrix as suggested by a nitrogen retention detected by EDS, a strong structural amorphization seen in XRD analysis and an intense Raman signal at 2328 cm^{-1}. Moreover, the c-axis cell parameter value of the annealed films, extracted from the XRD patterns, is also intermediate to those of the "as-deposited" oxynitride films and of the pristine powder.

Thermally oxidized at a low temperature ranging from 550°C to 650°C, SLTTON film can thus be described as perovskite-type intermediate phases with a nitrogen amount (≈ 9 at.%) compatible with a $SrTaO_{3.5}(N_2)_{0.25}$ typical composition (at.%N = 8.3) consistent with the TGA analysis previously conducted on $SrTaO_2N$ powder [22,28].

3. Dielectric characterization

The purpose of the present study was to achieve a stoichiometric composition for STLTO oxide films and to characterize the dielectric properties of samples with the aim to emphasize high tunabilities of their permittivity as what was pointed out for STLTO dense ceramics [8,12].

Annealings under air of stoichiometric oxynitride films has led to original film samples corresponding to intermediate phases between pure oxide and pure oxynitride, which still contain nitrogen in the form of N≡N pairs in an oxide matrix. It is then of interest to characterize their dielectric properties.

First of all, let's present in Figure 9 the evolution of the permittivity as a function of a DC electric field of the "STLTO as-deposited" film. At E = 0 and 10 kHz, this TTB-oxide film presents a permittivity value ε' = 139 with dielectric loss tanθ = 3.10-3. Moreover, these characteristics vary with the DC bias, with a tunability equal to T = 9 % at 310 kV/cm, 10 kHz and room temperature. Our TTB-STLTO-film is tunable but the present tunability value is far lower from the one measured on the perovskite-STLTO-ceramic with the composition x = 1.65 (T ≈ 55 % at 30 kV/cm [12]). Nevertheless, we note that the dielectric losses of this TTB oxide film are very low (tanθ = 3 10-3 at 310 kV/cm) which may be interesting in order to reduce the loss of insertion of a tunable antenna [35] based on this TTB material, for instance.

The oxynitride “STLTON as-deposited” sample has the following dielectric characteristics : at E = 0 and 10 kHz, ε '~ 2350 with very high losses tanθ ~ 3.5. These high values may be explained by the slight nitrogen over-stoechiometry evidenced by the EDS measurement (Nat% = 24.5, Table 3) which would cause the formation of polarizable defects in the structure of the materials leading to a high permittivity and high losses. Moreover, no electric field can be applied to this film as a high leakage current is observed as soon as the field is applied. Its permittivity meets those previously reported on other oxynitride films, $SrTaO_2N$ [36] and $LaTiO_2N$ [37] films for example. For the STLTON annealed films, dielectric measurements were performed on the STLTON-25 film annealed at TA = 600°C. Figure 10 presents the evolution as a function of a static electric field of its permittivity and dielectric loss tangent. Compared to the “as-deposited” STLTON sample, we noticed a notable evolution of its dielectric characteristics : at E = 0 and 10 kHz, the permittivity remains high (ε '~ 2200) but the losses have fallen sharply to tanθ ~ 0.07.

Moreover, we observe a variation of its permittivity with the DC bias, from ε '= 2200 to ε' = 1620, which corresponds to a tunability T = 26 % at 30 kV/cm. The associated dielectric loss tangent remain relatively constant, from tanθ ~ 0.07 to tanθ ~ 0.18 at 30 kV/cm. Beyond, the film no longer holds tension and losses rise away. In other words, the dielectric properties of the annealed STLTON films are intermediate as well between those of the TTB as-deposited oxide films (tunability and low losses) and those of the oxynitride films (high permittivity, no stability upon electric field). Looking for stoichiometric STLTO oxide films, we have obtained original intermediate phases which present very interesting dielectric characteristics with a high tunability (26 %) at a low bias (30 kV/cm). This tunability is much more higher than that obtained on the TTB STLTO film at the same bias (T = 0.01%). It is almost comparable to the tunability (T = 55 % at 30 kV/cm) obtained on a x = 1.65 STLTO ceramic [12] and so can be interesting from the moment the dielectric losses of the intermediate phase are lowered, for example by a second annealing during long times (several ten hours) at moderate temperatures (350 – 450°C).

4. Conclusion

The objective of the present work was to produce as thin films the x = 1.65 composition of the perovskite $(Sr_2Ta_2O_7)_{100-x}(La_2Ti_2O_7)x$ (STLTO) solid solution, exhibiting, as ceramics, optimum dielectric and ferroelectric properties. Deposition of thin films by rf magnetron sputtering of the oxide STLTO (x = 1.65) target under dioxygen reactive gas produces

systematically tetragonal tungsten bronze (TTB) films with Sr/Ta close to 0.55, thus denoting a high strontium deficiency in samples. The stoichiometric ratio can be achieved but in oxynitride STLTON films deposited using the same target under dinitrogen reactive gas. The post-annealing under air of the oxynitride films in the temperature range [450-1000°C] lead to transparent films still containing a certain amount of nitrogen. Raman experiments highlight the presence of nitrogen-nitrogen pairs embedded in a perovskite oxide matrix, thus identifying these annealed oxynitride films as intermediate phases already evidenced in powders. Dielectric measurements on a STLTON film annealed at 600°C during 4 h show a significant reduction of the dielectric losses to some 10-2, with a permittivity still at a high level close to 2000 (RT, 10 kHz). The tunability of this original compound is at a high level with a tunability value of 26 % at 30 kV/cm much more higher than that obtained on the TTB film at the same bias (T = 0.01%).

Acknowledgements

This work was supported by the European Union through the European Regional Development Fund (ERDF) and by the Ministry of Higher Education and Research, Brittany Région and Côtes d'Armor Département through the CPER Projects MATECOM and SOPHIE-STICC. This publication work was also supported by the Conseil Départemental des Côtes d'Armor, Saint Brieuc Armor Agglomération and the Syndicat de Gestion du Pole Universitaire de Saint Brieuc (France). Authors also thank the SIR platform of ScanMAT at University of Rennes 1 for technical assistance for the Raman measurements.

References

[1] M. Jansen, H.P. Letschert, Inorganic yellow-red pigments without toxic metals, Nature 404 (2000) 980.

[2] R. Marchand, F. Tessier, A. Le Sauze, N. Diot, Typical features of nitrogen in nitride-type compounds, Inter. J. Inorg. Mate. 3 (2001) 1143.

[3] A. Hosono, S.-K. Sun, Y. Masubuchi, S. Kikkawa, Additive sintering and post-ammonolysis of dielectric $BaTaO_2N$ oxynitride perovskite, J. Eur. Ceram. Soc. 36 (2016) 3341.

[4] C. Le Paven-Thivet, L. Le Gendre, J. Le Castrec, F. Chevire, F. Tessier, J. Pinel Oxynitride perovskite $LaTiO_xN_y$ thin films deposited by reactive sputtering, Progr. Solid State Chem.35 (2007) 299.

[5] W. Wang, M. O. Tadé, Z. Shao, Nitrogen-doped simple and complex oxides for photocatalysis : A review, Progr. Mater. Sci. 92 (2018) 33.

[6] N. Nishimura, R. Biet, K. Maeda, L. Le Gendre, R. Abe, J. Kubota, K. Domen, Effect of $TiCl_4$ treatment on the photoelectrochemical properties of $LaTiO_2N$ electrodes for water splitting under visible light, Thin Solid Films 518 (2010) 5855.

[7] A. Fuertes, Synthetic approaches in oxynitride chemistry, Progr. Solid State Chem. 51 (2018) 63.

[8] F. Marlec, C. Le Paven, F. Cheviré, L. Le Gendre, R. Benzerga, B. Guiffard, T. Dufay, F. Tessier, B. Messaid, A. Sharaiha, Ferroelectricity and high tunability in novel strontium and tantalum based layered perovskite materials, Jo. Eur. Ceram. Soc., 38 (2018) 2526.

[9] F. Lichtenberg, A. Herrnberger, K. Wiedenmann, J. Mannhart, Synthesis of Perovskite-Related Layered $A_nB_nO_{3n+2}$ = ABO_X type niobates and titanates and study of their structural, electric and magnetic properties, Progress in Solid State Chemistry 29 (2001) 1.

[10] A. Hushur, G. Shabbir, J-H. Ko, S. Kojima, The phase transitions of ferroelectric $Sr_2Ta_2O_7$ crystals by MDSC, Brillouin and dielectric spectroscopy, J. Phys. D: Appl. Phys. 37 (2004) 1127.

[11] H. Yan, H. Ning, Y. Kan, P. Wang, M. J. Reece, Piezoelectric Ceramics with Super-High Curie Points, J. Am. Ceram. Soc. 92 (2009) 2270.

[12] M. Haydoura, R. Benzerga, C. Le Paven, V. Laur, A. Chevalier, L. Le Gendre, Y. Bai, H. Jantunen, F. Marlec, A. Sharaiha, Dielectric characterization in low and high frequencies of new ferroelectric strontium and tantalum based perovskite ceramics, E-MRS 2019 Spring Meeting, Nice (France), May 27 - 31, 2019.

[13] C. Le Paven-Thivet, A. Ishikawa, A. Ziani, L. Le Gendre, M. Yoshida, J. Kubota, F. Tessier, K. Domen, Photoelectrochemical properties of crystalline perovskite lanthanum titanium oxynitride films under visible light, J. Phys. Chem. C 113 (2009) 6156.

[14] A. Ziani, C. Le Paven, L. Le Gendre, F. Marlec, R. Benzerga, F. Tessier, F. Cheviré, M. N. Hedhili, A. T. Garcia-Esparza, S. Melissen, P. Sautet, T. Le Bahers, K. Takanabe, Photophysical properties of $SrTaO_2N$ thin films and influence of anion ordering : a joint theoretical and experimental investigation, Chem. Mater. 29 (2017) 3989.

[15] D. Oka, Y. Hirose, H. Kamisaka, T. Fukumura, K. Sasa, S. Ishii, H. Matsuzaki, Y. Sato, Y. Ikuhara, T. Hasegawa, Possible ferroelectricity in perovskite oxynitride $SrTaO_2N$ epitaxial thin film, Sci. Rep. 16 (2014) 4987.

[16] Y. Lu, C. Le Paven-Thivet, H. Nguyen, R. Benzerga, L. Le Gendre, S. Rioual, F. Tessier, F. Cheviré, A. Sharaiha, C. Delaveaud, X. Castel, Reactive sputtering deposition of perovskite oxide

and oxynitride lanthanum titanium films : structural and dielectric characterization, Crystal Growth & Design 13 (2013) 4852.

[17] H.-N. Nguyen, R. Benzerga, C. Delaveaud, C. Le Paven-Thivet, Y. Lu, A. Sharaiha, L. Le Gendre, S. Députier, F. Tessier, F. Cheviré, X. Castel, Miniaturized notch antenna based on lanthanum titanium perovskite oxide thin films, Thin Solid Films 563 (2014) 36.

[18] F. Marlec, C. Le Paven, L. Le Gendre, R. Benzerga, F. Cheviré, F. Tessier, F. Gam, A. Sharaiha, Deposition and dielectric study as function of thickness of perovskite oxynitride $SrTaO_2N$ thin films elaborated by reactive sputtering, Surf. Coat. Tech. 324 (2017) 607.

[19] C. Baristiran Kaynak, M. Lukosius, I. Costina, B. Tillack, Ch. Wenger, G. Ruhl, T. Blomberg, Enhanced leakage current behavior of $Sr_2Ta_2O_{7-x}/SrTiO_3$ bilayer dielectrics for metal-insulator-metal capacitors, Thin Solid Films 519 (2011) 5734.

[20] L. Le Gendre, R. Marchand, Y. Laurent, A new class of inorganic compounds containing dinitrogen – metal bounds, J. Eur. Ceram. Soc. 17 (1997) 1813.

[21] L. Le Gendre, R. Marchand, B. Piriou, Raman scattering investigations of dinitrogen entities in oxidized $LaTiO_2N$ perovskite, Eur. J. Solid State Inorg. Chem. 34 (1997) 973.

[22] A. Rachel, S.G. Ebbinghaus, M. Güngerich, P.J. Klar, J. Hanss, A. Weidenkaff, A. Reller, Tantalum and niobium perovskite oxynitrides : Synthesis and analysis of the thermal behavior, Thermochimica Acta 438 (2005) 134.

[23] D. Kubelka, L. Munk, Ein beitrag zur optik der farbanstriche, Z. Tech. Phys. 12 (1931) 593.

[24] E. Lee, C.H. Park, D. P. Shoemake, M. Avdeev, Y.-Il Kim, Crystal structure analysis of tungsten bronzes β-$SrTa_2O_6$ and β'-$SrTa_2O_6$ by synchrotron X-ray and neutron powder diffraction, J. Solid State Chem. 191 (2012) 232.

[25] S.G. Ebbinghaus, H-P. Abicht, R. Dronskowski, T. Müller, A. Reller, A. Weidenkaff, Perovskite-related oxynitrides : recent developments in synthesis, characterisation and investigations of physical properties, Progr. Solid State Chem. 37 (2009) 173.

[26] S.J. Clarke, C.W. Michie, M.J. Rosseinsky, Structure of Zr_2ON_2 by Neutron Powder Diffraction : The Absence of Nitride–Oxide Ordering, J. Solid State Chem. 146 (1999) 399.

[27] N. Kumar, A. Sundaresan, C.N.R. Rao, Rare earth niobium oxynitrides, $LnNbON_{2-\delta}$ (Ln = Y, La, Pr, Nd, Gd, Dy): Synthesis, structure and properties, Mat. Res. Bull. 46 (2011) 2021.

[28] R. Aguiar, D. Logvinovich, A. Weidenkaff, A. Rachel, A. Reller, S. G. Ebbinghaus, The vast colour spectrum of ternary metal oxynitride pigments, Dyes and Pigments 76 (2008) 70.

[29] Sierra Gallego, N. Marin Alzate, O, Arnache, A novel $LaFeO_{3-x}N_x$ oxynitride : Synthesis and characterization, J. Alloys Comp. 549 (2013) 163.

[30] A. Maegli, S. Yoon, E. Otal, L. Karvonen, P. Mandaliev, A. Weidenkaff, Perovskite-type $SrTi_{1-x}Nb_x(O,N)_3$ compounds: Synthesis, crystal structure and optical properties, J. Solid State Chem. 184 (2011) 929.

[31] J.W.H. van Krevel, H. T. Hintzen , R. Metselaar, L. Le Gendre, R. Marchand, Oxidation resistance of Ln-Si-O-N powders, Solid State Sci. 3 (2001) 49.

[32] G. Tobias , J. Oro-Sole, D. Beltran-Porter, A. Fuertes, Synthesis and crystal structure of novel Ruddlesden–Popper strontium niobium oxynitrides, Crystal Eng. 5 (2002) 479.

[33] P. Goursat, M. Billy, P. Goeuriot, J.C. Labbe, J.M. Villechenoux, G. Roult, J. Bardolle, Contribution à l'étude du système Al/0/N II: rétention d'azote dans les produits d'oxydation de l'oxynitrure d'aluminium γ, Mater. Chem. 6 (1981) 81.

[34] F. Tessier, L. Le Gendre, F. Cheviré, R. Marchand, A. Navrotsky, Thermochemistry of a New Class of Materials Containing Dinitrogen Pairs in an Oxide Matrix, Chem. Mater. 17 (2005) 3570.

[35] H. V. Nguyen, R. Benzerga, C. Borderon, C. Delaveaud, A. Sharaiha, R. Renoud, C. Le Paven, S. Pavy, K. Nadaud, H. W. Gundel, Miniaturized and reconfigurable notch antenna based on a BST ferroelectric thin film, Materials Research Bulletin 67 (2015) 255.

[36] D. Oka, Y. Hirose, H. Kamisaka, T. Fukumura, K. Sasa, S. Ishii, H. Matsuzaki, Y. Sato, Y. Ikuhara, T. Hasegawa, Possible ferroelectricity in perovskite oxynitride $SrTaO_2N$ epitaxial thin films, Sci. Rep. 4 (2014) 4987.

[37] A. Ziani, C. Le Paven-Thivet, L. Le Gendre, D. Fasquelle, J.C. Carru, F. Tessier, J. Pinel, Structural and dielectric properties of oxynitride perovskite $LaTiO_xN_y$ thin films, Thin Solid Films 517 (2008) 544.

Figure Captions

Figure 1. θ-2θ XRD diagram of the $(Sr_2Ta_2O_7)_{98.35}(La_2Ti_2O_7)_{1.65}$ target (hereafter named as "Pristine STLTO powder") used for the deposition of thin films by reactive radio-frequency magnetron sputtering (indexation according to $Sr_2Ta_2O_7$).

Figure 2. (a) UV-visible transmittance spectra and (b) curves for the determination of the band gap values of the "STLTO as-deposited" and "STLTON as-deposited" films deposited by reactive rf magnetron sputtering with, respectively, $\%O_2 = 25$ and $\%N_2 = 25$.

Figure 3. Evolution as a function of the reactive gas (O_2 or N_2) percentage in the sputtering plasma of the Sr/Ta ratio of STLTO and STLTON films deposited by reactive rf magnetron sputtering.

Figure 4. θ-2θ XRD diagrams of the STLTO and STLTON "as-deposited" films on MgO substrates by reactive rf magnetron sputtering (indexation according to $Sr_{2,83}Ta_5O_{15}$ for STLTO and to $SrTaO_2N$ for STLTON)

Figure 5. Evolution as a function of the dioxygen percentage in the reactive sputtering gas of the out-of-plane c parameter of STLTO thin films.

Figure 6: (a) Complete θ-2θ XRD diagrams of STLTON thin films annealed under air during 4 h at different annealing temperatures. Comparison is made to that of STLTON and STLTO as-deposited films and pristine STLTO powder (b) details between 40 and 50° (the orange and blue dotted lines are a visual cue for the oxynitride and oxide positions, respectively, while the annealed films are marked by a grey line ; * sample holder).

Figure 7. Evolution as a function of the annealing temperature (TA) of the cell parameter c of annealed-STLTON thin films. Their characteristics are compared to that of STLTON asdeposited film and STLTO pristine powder.

Figure 8. Raman spectra in the [2300-2350]cm^{-1} range of the bare MgO substrate, the asdeposited STLTON-25 oxynitride film and the STLTON-25 film annealed under air at 600°C during 4 h.

Figure 9. Evolution as a function of a static electric field of the permittivity (ε') and the dielectric loss tangent (tanθ) of: (a) the oxide STLTO "as-deposited".

Figure 10. Evolution as a function of a static electric field of the permittivity (ε') and the dielectric loss tangent (tanθ) of the STLTON film annealed at TA = 600°C.

Table 1: List of STLTO films deposited by rf magnetron sputtering with different percentages of reactive dioxygen gas, along with the cationic composition (ratio Sr/Ta), the band gap (Eg) and the thickness of samples.

Table 2: List of STLTON films deposited by rf magnetron sputtering with different percentages of reactive dinitrogen gas, along with the cationic composition (ratio Sr/Ta) and the band gap (Eg).

Table 3: List of samples of interest for the annealing of STLTON film, along with the cationic composition (ratio Sr/Ta), the nitrogen content and the anionic composition (O/N), determined by EDS, and the band-gap Eg measured by UV-Visible Transmittance.

Table1

	$\%O_2$ (vol.) during deposition	Cationic composition Sr/Ta	Band gap Eg (eV)	Thickness (nm)
STLTO-5	**5**	0.54	3,2	1050
STLTO-10	**10**	0.55	4.5	870
STLTO-25	**25**	0.51	4.3	960
STLTO-50	**50**	0.53	4.4	1100
STLTO-75	**75**	0.53	4.4	880

Table2

	$\%N_2$ (vol.) during deposition	Cationic composition Sr/Ta	Band gap Eg (eV)
STLTON-5	**5**	0.94	2.2
STLTON-10	**15**	0.95	-
STLTON-25	**25**	0.99	2.3
STLTON-50	**50**	1.06	2.4
STLTON-75	**75**	1.07	2.4

Table3

	Annealing temperature T_A (°C)	Cationic composition Sr/Ta	Nitrogen content (at.%N)	Anionic composition O/N	Band gap Eg (eV)
STLTO	**Pristine powder**	0.98	-	-	-
STLTO-25	**As-deposited**	0.51	-	-	4.3
STLTON-25	**As-deposited**	1.00	24.5	1.7	2.3
STLTON-25 annealed	**450**	-	-	-	2.5
	550	1.14	9.5	7.2	4.5
	600	0.88	9.0	7.6	4.6
	650	1.11	8.5	7.3	4.1
	1000	0,95	0	-	-

Figure1

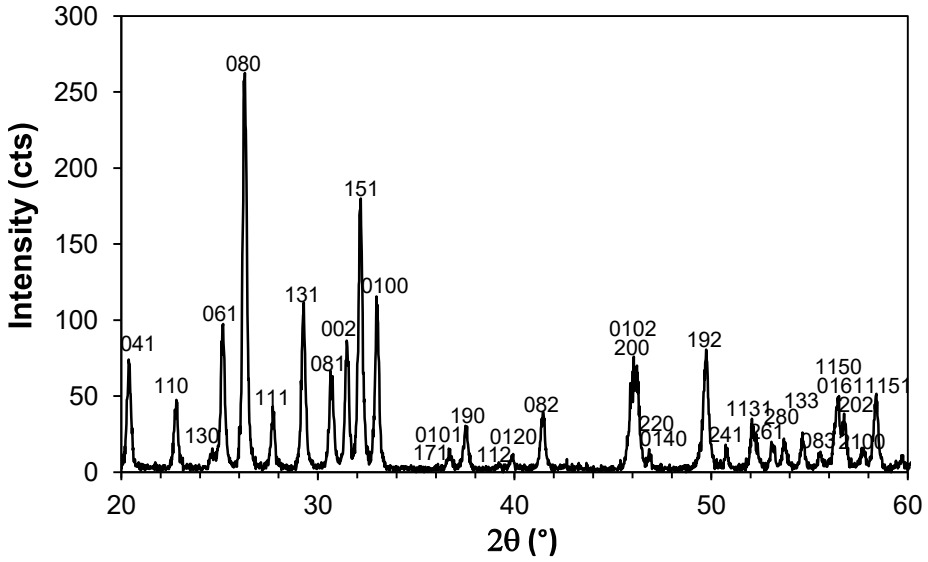
Intensity (cts)
2θ (°)
300
250
200
150
100
50
0
20
30
40
50
60
041
110
130
061
080
111
131
081
002
151
0100
171
0101
190
112
0120
082
0102
200
220
0140
192
241
1131
261
280
133
083
1150
01611
202
2100
1151

Figure2

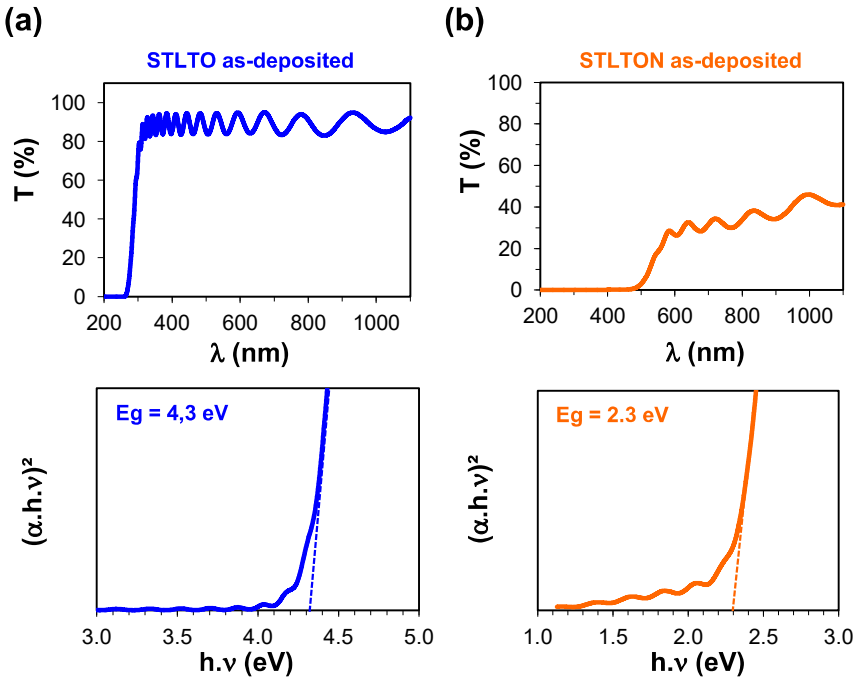
(a)
STLTO as-deposited
T (%)
λ (nm)
Eg = 4,3 eV
(α.h.ν)²
h.ν (eV)
(b)
STLTON as-deposited
T (%)
λ (nm)
Eg = 2.3 eV
(α.h.ν)²
h.ν (eV)

Figure3

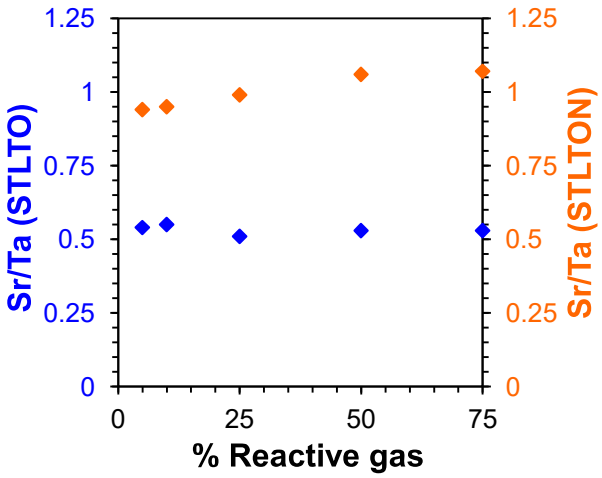
1.25
1
0.75
0.5
0.25
0
Sr/Ta (STLTO)
1.25
1
0.75
0.5
0.25
0
Sr/Ta (STLTON)
0
25
50
75
% Reactive gas

Figure4

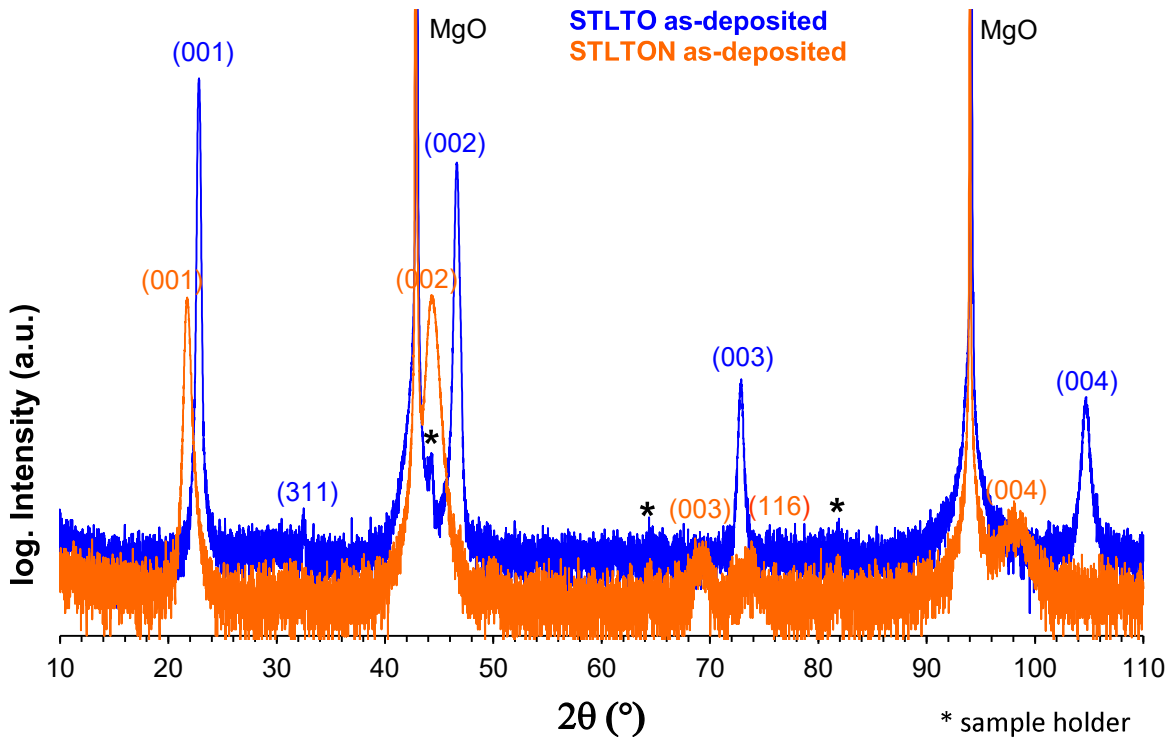
STLTO as-deposited
STLTON as-deposited
MgO
MgO
(001)
(002)
(001)
(002)
(003)
(004)
(311)
(003)
(116)
(004)
*
*
*
log. Intensity (a.u.)
10
20
30
40
50
60
70
80
90
100
110
2θ (°)
* sample holder

Figure5

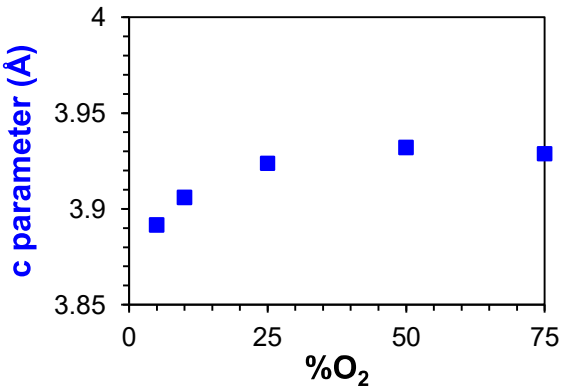

Figure6

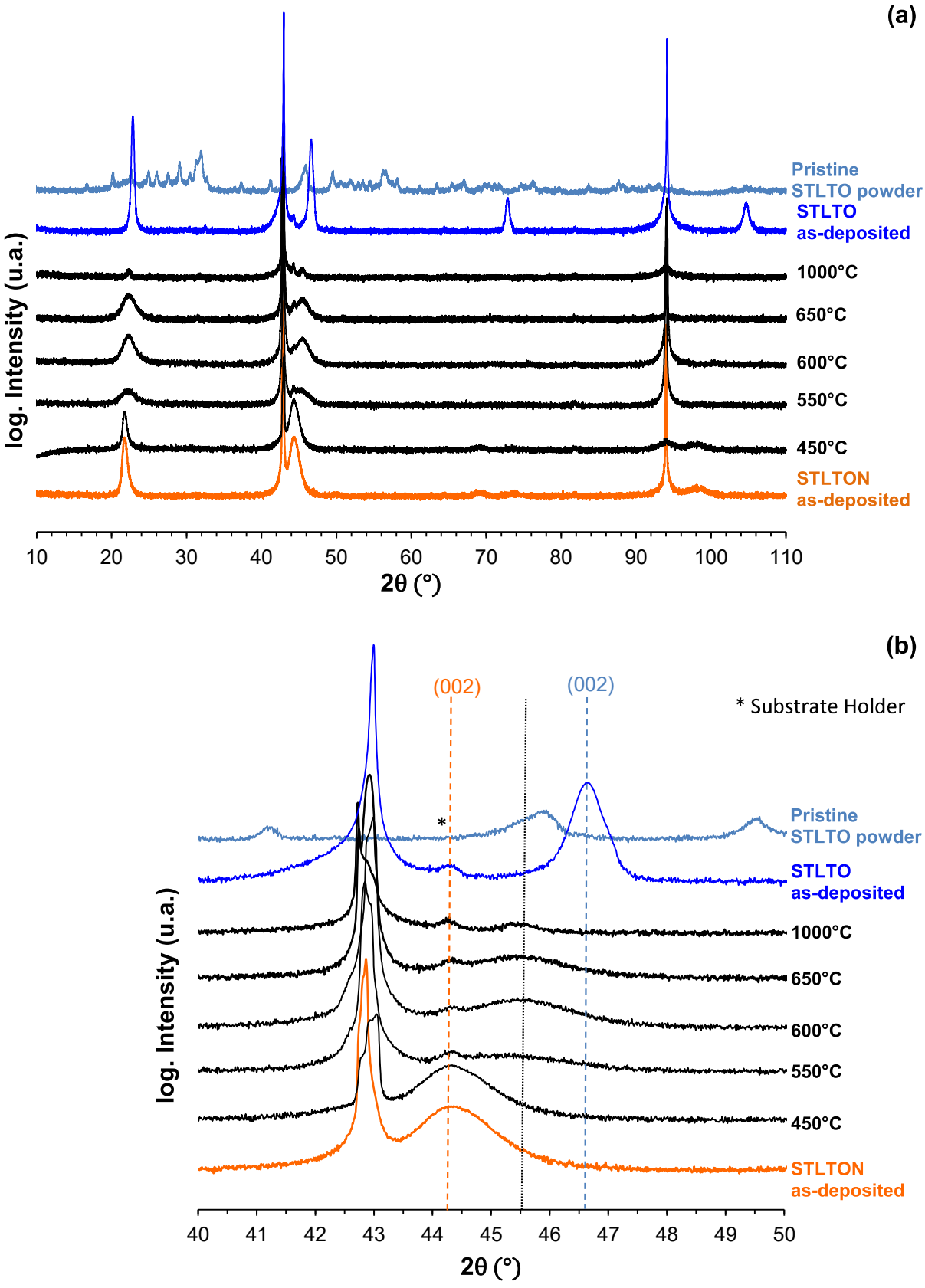
(a)
log. Intensity (u.a.)
Pristine STLTO powder
STLTO as-deposited
1000°C
650°C
600°C
550°C
450°C
STLTON as-deposited
10 20 30 40 50 60 70 80 90 100 110
2θ (°)
(b)
(002)
(002)
* Substrate Holder
*
log. Intensity (u.a.)
Pristine STLTO powder
STLTO as-deposited
1000°C
650°C
600°C
550°C
450°C
STLTON as-deposited
40 41 42 43 44 45 46 47 48 49 50
2θ (°)

Figure7

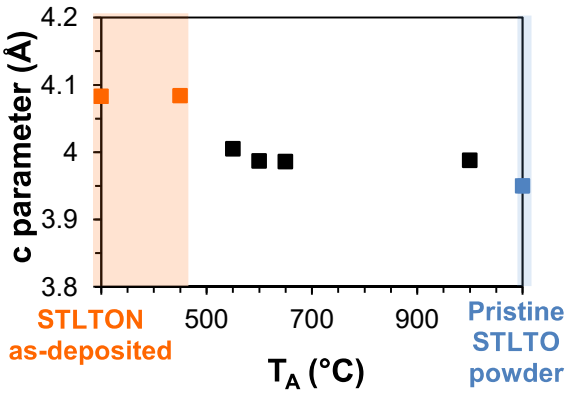
4.2
4.1
4
3.9
3.8
c parameter (Å)
STLTON
as-deposited
500
700
900
Pristine
STLTO
powder
T_A (°C)

Figure8

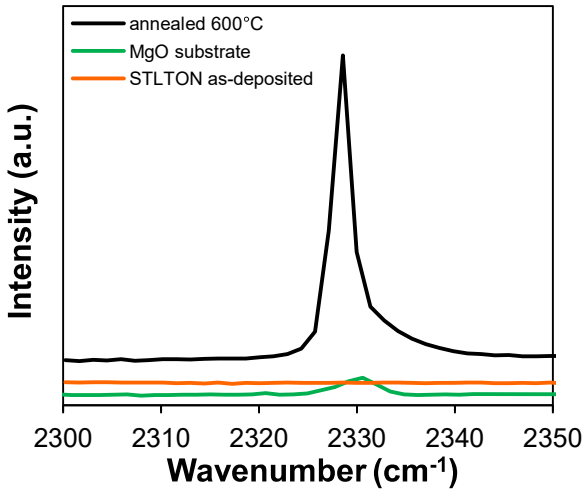
annealed 600°C
MgO substrate
STLTON as-deposited
Intensity (a.u.)
2300
2310
2320
2330
2340
2350
Wavenumber (cm-1)

Figure9

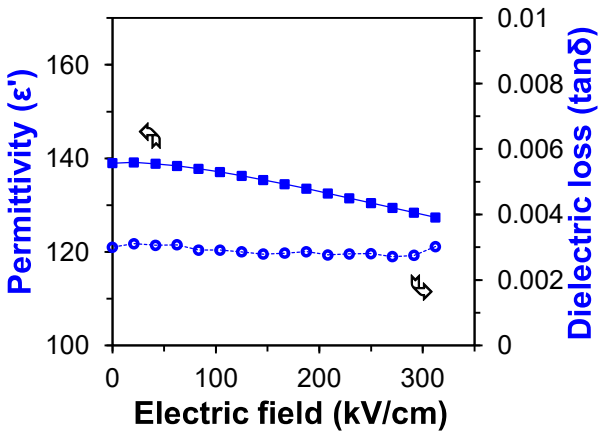
Permittivity (ε')
160
140
120
100
0.01
0.008
0.006
0.004
0.002
0
Dielectric loss (tanδ)
0
100
200
300
Electric field (kV/cm)

Figure10

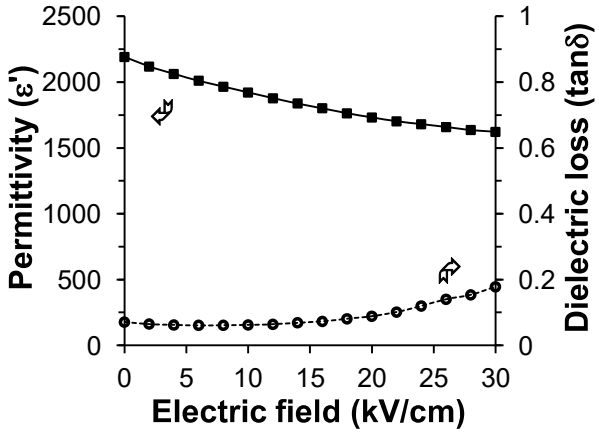
Permittivity (ε')
Dielectric loss (tanδ)
Electric field (kV/cm)
2500
2000
1500
1000
500
0
1
0.8
0.6
0.4
0.2
0
0
5
10
15
20
25
30